

Electron beam driven generation of relativistic sub-cycle pulses from infrared to ultraviolet frequencies

I. Thiele,^{1,*} E. Siminos,² and T. Fülöp¹

¹*Department of Physics, Chalmers University of Technology, SE-412 96 Göteborg, Sweden*

²*Department of Physics, University of Gothenburg, SE-412 96 Göteborg, Sweden*

(Dated: September 10, 2022)

We propose a novel scheme of isolated relativistic infrared to extreme ultraviolet sub-cycle electromagnetic pulse generation. To this end a pump electron beam is injected into an electromagnetic seed pulse as the latter is reflected by a mirror. The electron beam is shown to be able to amplify the field of the seed pulse while upshifting its central frequency and reducing its number of cycles. We demonstrate the amplification by means of 1D and 2D particle-in-cell simulations. In order to explain and optimize the amplification process, a model based on fluid theory is proposed. We estimate that using currently available electron beams and terahertz pulse sources, our scheme is able to produce mJ-strong mid-infrared sub-cycle pulses.

Generation of few cycle electromagnetic pulses has steadily advanced, driven by applications which require probing or control of ultra-fast processes [1, 2]. Recently a lot of effort has been devoted to producing sub-cycle pulses in which the time-envelope is modulated at time scale shorter than a single cycle. Such pulses bring temporal resolution to its ultimate limits and are unique tools for the control of electron motion in solids [3], electron tunneling in nano-devices [4], reaction dynamics at the electronic level [5], as well as the generation of isolated attosecond and zeptosecond X-ray pulses [6]. Several methods like optical synthesis or parametric amplification have been developed for the generation of sub-cycle pulses from the THz to X-ray regimes (see the review [7]). However, scaling such methods towards high intensities remains challenging and thus a field of active research, in particular in the mid-infrared regime where intense sub-cycle pulses are very attractive for applications [8]. The main limitation of the typically used parametric amplification methods is the material damage threshold under intense fields [9]. On the other hand, methods exploiting plasmas or electron beams as a frequency conversion medium, such as high-harmonic generation from solid targets [10], Thomson scattering amplification [11], scattering by relativistic mirrors [12] and frequency down-conversion in a plasma wake [13] are not subject to a damage threshold. However, these methods are not able to generate isolated sub-cycle pulses.

In this letter, we propose a method to generate isolated sub-cycle pulses reaching relativistic intensities. As visualized in Fig. 1, our scheme involves the interaction of a seed electromagnetic pulse with a short duration pump electron beam at a thin foil. The thin foil acts as a mirror reflecting the seed pulse, while the electron beam enters in the middle of the pulse and leads to its amplification in a co-propagating configuration. Scaling the energy of the electron beam and electromagnetic pulse is not subject to some damage threshold making our scheme strongly up-scalable as will be shown below. Contemporary laser-

wakefield accelerators can provide fs-short 200-MeV electron beams with hundreds of pC beam charge and thus tens to hundreds of mJ beam energy [14]. Transferring a substantial part of this energy can lead to mJ-strong relativistic sub-cycle pulses.

We demonstrate the scheme through a 2D particle-in-cell (PIC) simulation with the code SMILEI [15]. A linearly polarized single-cycle seed pulse is focused strongly onto a thin almost perfectly reflecting foil. Such single-cycle pulses can be easily produced in the THz domain [16]. However, as will be clarified later on, our scheme can also operate with many-cycle seed pulses. The incoming seed pulse is focused at the mirror to a Gaussian focal spot with $1/e$ -beam width $y_0 = 0.3\lambda_0$, Gaussian time-envelop with $1/e$ -duration $t_0 = 0.21T_0$, a sine-like carrier with frequency $\omega_0 = 2\pi/T_0$ and corresponding wavelength λ_0 for the y -polarized electric field of amplitude $E_0^{\text{in}} = E_c$, where $E_c = cm_e\omega_0/q_e$. The electron beam is entering from the back side of

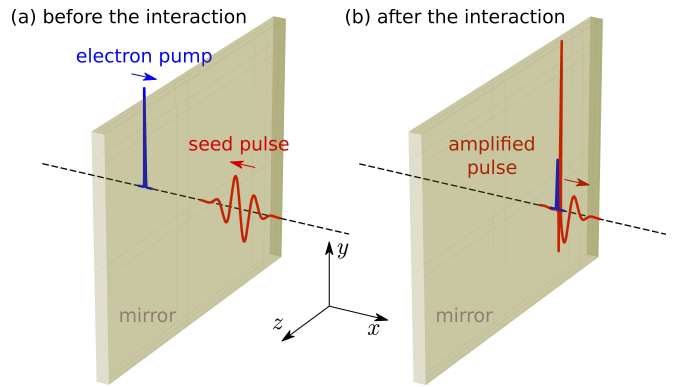


FIG. 1. Schematic representation of the electron beam driven amplification scheme: (a) The counter-propagating seed electromagnetic pulse and pump electron beam are moving towards a mirror (thin foil). (b) The electromagnetic pulse is reflected by the mirror and interacts with the electron beam as it exits through the mirror, leading to the generation and amplification of an intense sub-cycle pulse.

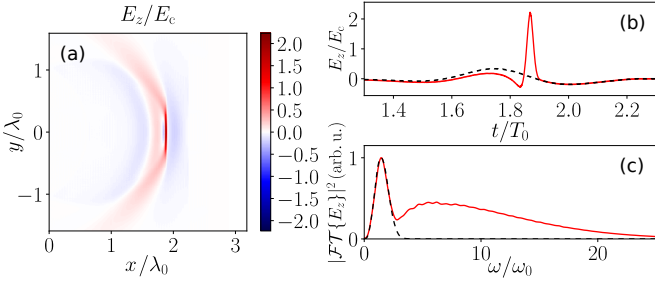


FIG. 2. (a) Electric field snapshot after the interaction of a strongly focused low-frequency pulse with an electron beam passing the standing mirror at $x = 0$. Corresponding on-axis signal (b) and spectrum (c) demonstrating the generation of an intense higher-frequency sub-cycle pulse (solid red lines). Corresponding signals without the electron beam (dashed black lines). The parameters are: $t_e = 0.016T_0$, $y_0 = 0.3\lambda_0$, $n_e^{\max} = 28.3n_c$, $\gamma_e = 20$, $t_0 = 0.21T_0$ and $E_0^{\text{in}} = E_c$, where $E_c = cm_e\omega_0/q_e$. The simulation was performed with 1600 points per electromagnetic pulse carrier wavelength along x , 100 points along y and 1608 points per electromagnetic pulse carrier oscillation. For every species 100 particles per cell were used. The mirror has been modeled as a dense electron-proton plasma with thickness $1.4c/\omega_0$.

the foil. It is initialized with a constant gamma factor $\gamma_e = 20$ and a Gaussian density profile with $1/e$ -thickness $y_0 = 0.3\lambda_0$, duration $t_e = 0.016T_0$ and peak density $n_e^{\max} = 28.3n_c$, where $n_c = m_e\epsilon_0\omega_0^2/q_e^2$ is the critical density for a resting plasma. A snapshot of the electric field after the amplification process has been completed is presented in Fig. 2(a). We observe a strong sub-cycle pulse around $x = 1.91\lambda_0$. It is well collimated compared to the residual driving electromagnetic pulse which diffracts strongly due to the tight focusing. This is an advantageous property of the scheme because of the natural separation between the seed and amplified electromagnetic pulse. As the on-axis electric field time-trace in Fig. 2(b) demonstrates, already after propagation for two seed-wavelengths, the pulses are almost separated. The corresponding frequency spectrum in Fig. 2(c) shows that the generated sub-cycle pulse is up-shifted by a factor of seven in terms of peak frequency and is therefore diffracting much less than the seed pulse.

In order to illustrate why a standing mirror is required in addition to the electron beam in order to produce *sub-cycle* pulses, we consider the simplified space-time diagrams of Fig. 3. We restrict attention to 1D geometry and consider the limit of an infinitely dense and sharply rising electron beam front. Without the standing mirror [Fig. 3(a)] the setup is known as the relativistic flying mirror concept [12]. The solid red line indicates the edges of the incoming electromagnetic pulse which is perfectly reflected by the electron beam. Due to the double Doppler shift effect the frequency of the reflected pulse is upshifted and its amplitude amplified by a factor $\approx 4\gamma_e^2$ [17]. While the duration of the reflected pulse is

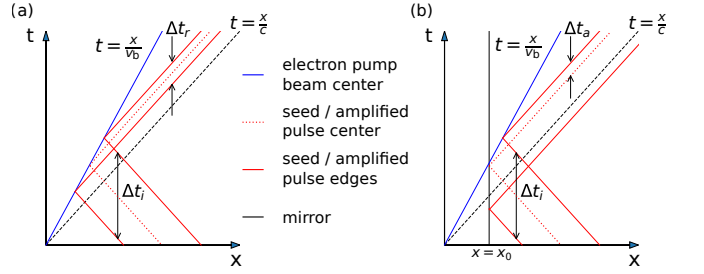


FIG. 3. Space-time diagrams visualizing the electron beam (blue line) moving with speed v_b and electromagnetic pulse (red lines) without (a) or with (b) the standing mirror at $x = x_0$ [black line in (b)]: Without the mirror the whole electromagnetic pulse and with the mirror only part of the electromagnetic pulse interacts with the electron beam allowing for sub-cycle pulse generation.

shortened by the same factor, the number of cycles remains invariant. By contrast, when the standing mirror is introduced [solid black line at $x = x_0$ in Fig. 3(b)], the leading part of the electromagnetic pulse is simply reflected and not amplified. Only the trailing part interacts with the electron beam and, thus, the number of *amplified* cycles is reduced.

In Fig. 4, these two situations are compared through the use of 1D PIC simulations for few-cycle driving electromagnetic pulses interacting with electron bunches of realistic density profiles. As expected, without the mirror [Fig. 4(a)] the number of cycles is conserved, i.e., no generation of sub-cycle pulses is possible. The reflected pulse contains only 1.7 % of the initial electromagnetic pulse energy, it is much shorter and has an amplitude diminished by 20 times compared to the incoming pulse. By contrast, with the mirror a strong sub-cycle pulse is generated [Fig. 4 (b)] with an amplitude exceeding the one of the incoming pulse by four times and the total energy doubled compared to the initial energy.

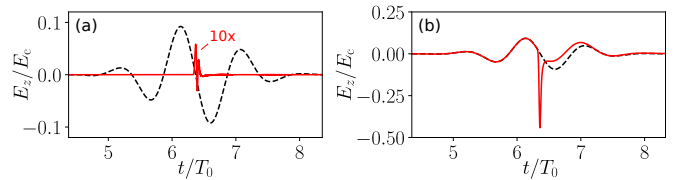


FIG. 4. Electric field time-traces before (dashed lines) and after (solid lines) the interaction using a few-cycle seed pulse and an underdense electron beam without (a) or with (b) the mirror. The field after the interaction without the mirror [solid line in (a)] has been magnified by a factor of 10 for a better comparison. The parameters are: $t_e = 0.016T_0$, $n_e^{\max} = 5.66n_c$, $\gamma_e = 10$, $t_0 = 0.85T_0$, $E_0^{\text{in}} = 0.1E_c$. The simulations were performed with 1600 points per electromagnetic pulse carrier wavelength and with 1000 particles per cell. The mirror has been modeled as a dense electron-proton plasma with thickness $0.22\lambda_0$.

We now develop a simplified fluid model of the interaction in order to illuminate the mechanism of amplification. In 1D ($\partial_z = \partial_y = 0$), the transverse fluid momentum \mathbf{p}_\perp evolves according to

$$\partial_t \mathbf{p}_\perp = q_e \mathbf{E}_\perp, \quad (1)$$

where \mathbf{E}_\perp is the transverse electric field, and q_e is the electron charge. This leads to conservation of transverse canonical momentum, $\mathbf{p}_\perp = -q_e \mathbf{A}_\perp/c$, where $\mathbf{A}_\perp = -\partial_t \mathbf{E}_\perp$ is the vector potential (in the Coulomb gauge). The transverse current reads

$$\mathbf{J}_\perp = (q_e/m_e) \mathbf{p}_\perp n_e / \gamma_e, \quad (2)$$

where $\gamma_e = \sqrt{1 + |\mathbf{p}|^2/(m_e c)^2}$, m_e is the electron mass and c the speed of light in vacuum. If we choose a sufficiently weak seed pulse, the longitudinal momentum of the electrons dominates and $\gamma_e \approx p_x/(m_e c)$. This allows us to neglect the effect of the seed pulse on the longitudinal electron beam momentum, i.e., to employ an undepleted pump beam approximation (UPBA). Equation (1) is then solved together with Maxwell's equations with a source term given by Eq. (2) for a given electron beam dynamics with prescribed $n_e(x, t)$ and $v_x(x, t) = p_x(x, t)/[m_e \gamma_e(x, t)]$. For simplicity we assume a density profile moving with a constant speed v_b ,

$$n_e(x, t) = n_e^{\max} \exp [-(t - t_d - x/v_b)^2/t_0^2], \quad (3)$$

with some delay t_d . The seed pulse arriving from $x = +\infty$ is perfectly reflected by the mirror at $x = 0$, i.e., the electric field at the mirror is zero. The fields can be decomposed into forward and backward propagating parts E_z^- and E_z^+ respectively such that the seed pulse electric field at the mirror is defined by

$$E_z^\pm(t) = \mp E_z^{\max} \sin(\omega_0 t) \exp(-t/t_0^2). \quad (4)$$

In Fig. 5(a), an example of a n_e/γ_e -profile (dotted line) and an outgoing seed electric field (dashed line) is shown.

The solution of the fluid model for a weak seed pulse and a density profile shorter than the cycle duration is shown in Fig. 5(b). We indeed observe a partial amplification of the incoming seed pulse (dashed line), leading to the formation of a sub-cycle pulse in the center of the original pulse. After the interaction, the pulse energy increases by a factor of 10 and the maximum electric field of the electromagnetic pulse is enhanced by about a factor of 14 (solid line). We compare the result of the fluid model with a PIC simulation [dark red solid line in Fig. 5(b)] to find an excellent agreement which justifies the use of the fluid picture and the UPBA. As Fig. 5(c) shows, the spectrum of the reflected pulse is up-shifted by a factor of seven and strongly broadened.

From Poynting's theorem and Eqs. (1) and (2) we can compute the energy density U_{gain} transferred to the electromagnetic field at any given point in space during the

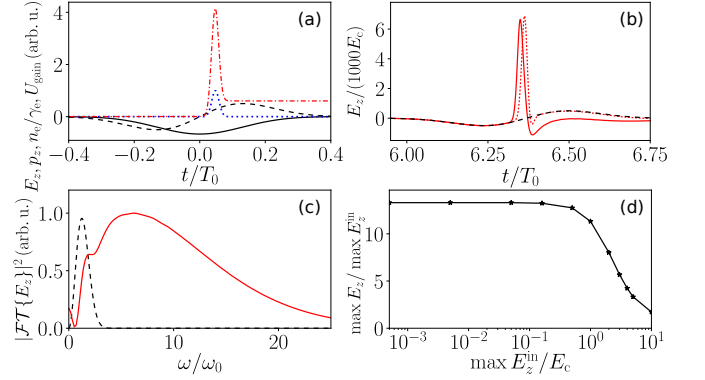


FIG. 5. (a) Visualization of the amplification mechanism: electric field approximated by the unperturbed reflected seed pulse field (dashed line), corresponding vector potential (solid line), electron density (dotted line) and time-dependent energy density gain U_{gain} (dash-dotted line). (b) Electric field after the interaction of the incoming plane wave single-cycle pulse (dashed line) with the electron beam according to the fluid model (dotted line) and PIC (solid line). (c) Spectra according to PIC simulation. The parameters are: $t_e = 0.016T_0$, $n_e^{\max} = 28.3n_c$, $\gamma_e = 20$, $t_0 = 0.21T_0$, $E_0^{\text{in}} = 0.001E_c$. The distance from the mirror to the detector is $6.37c/\omega_0$. (d) Peak electric field amplitude amplification for different incoming seed pulse amplitudes according to PIC simulations. The remaining parameters are the same as above.

interaction as

$$U_{\text{gain}}(t) = \frac{q_e^2}{2m_e c^2} \int_{-\infty}^t |\mathbf{A}_\perp|^2 \frac{\partial}{\partial \tau} \left(\frac{n_e}{\gamma_e} \right) d\tau. \quad (5)$$

Here we ignored terms that identically vanish after the end of the interaction. It is important to note that the sign of U_{gain} at any given time only depends on the rate of change of n_e/γ_e . For a constant γ_e , the rising part of the electron beam gives a gain, while the descending part of the electron beam gives a loss. Assuming a symmetric electron beam profile, a net gain after the end of the interaction ($t \rightarrow \infty$) requires an asymmetry in the amplitude of electromagnetic field vector potential $|\mathbf{A}_\perp|$.

A great advantage of our scheme (see Fig. 1) is that the introduction of the standing mirror allows the electron beam to be injected into the seed pulse in a way that such an asymmetry, and thus a net gain, can be achieved. This is illustrated in Fig. 5(a) where, in order to explain the interaction in simple terms, we assumed the electric field E_z to be the one of the unperturbed reflected seed pulse (dashed line). The corresponding transverse vector potential $\mathbf{A}_\perp = -c/q_e \mathbf{p}_\perp$ for our example can be then directly computed from Eq. (1) and is also presented in Fig. 5(a) (solid line). This gives the evolution of U_{gain} (dash-dotted line), which first increases at the rising edge of n_e/γ_e [dotted line in Fig. 5(a)] and then decreases at the descending edge. Since in our example we have chosen a slightly positive electron beam delay

t_d , a final local nonzero energy gain can be expected. We shall note that injecting the beam with $t_d = 0$ will also lead to an energy gain after some propagation since the electron beam is slower than the seed pulse.

For electron beam duration that is much shorter than the laser cycle we may Taylor-expand $\mathbf{A}_\perp(x, t)$ in Eq. (5) around $t = t_d$

$$U_{\text{gain}}(+\infty) = -\frac{q_e^2}{2m_e c^2} \frac{\partial}{\partial t} |\mathbf{A}_\perp(t_d)|^2 \int_{-\infty}^{+\infty} n_e/\gamma_e dt. \quad (6)$$

This shows explicitly the dependence of the energy gain on the electromagnetic field profile when the bunch exits through the mirror. We see that, in this limit, the maximum energy gain is independent of the electron beam duration for a constant charge. On the other hand, for an electron beam much longer than the wavelength, $|\mathbf{A}_\perp(t)|^2$ contributions in Eq. (5) cancel each other, diminishing the amplification effect.

The fluid model, within the UPBA, predicts a linear increase of the amplification with the amplitude of the seed pulse. As Fig. 5(d) shows, this is true up to relativistic seed pulse amplitudes. This feature of our scheme implies the possibility to up-scale the amplitudes of the amplified sub-cycle pulses up to relativistic intensities.

As the example in Fig. 4 demonstrates, our sub-cycle-pulse generation and amplification scheme works not only for single-cycle but also for few-cycle driving electromagnetic pulses. Actually, the scheme would lead to amplification for any duration of the driving pulse. As long as the electron beam duration is small compared to electromagnetic pulse cycle duration $2\pi/\omega_0$, Eq. (6) predicts a potential energy gain independent on the number of cycles in \mathbf{A}_\perp .

The cases demonstrated in Fig. 4 and Fig. 5 differ in terms of the maximum value for n_e/γ_e . In the latter case, the electron beam is overdense ($n_e^{\text{max}}/\gamma_e > n_c$) for the carrier frequency ω_0 , while in the former case it is underdense ($n_e^{\text{max}}/\gamma_e < n_c$), i.e., the reflectivity due to the electron beam itself is almost zero. Nevertheless, due to the mirror the incident electromagnetic pulse is fully reflected and an amplification by a factor of 4.8 is achieved even in the underdense case.

Finally, a few practical aspects are discussed. Up to now we presented our results in normalized units: in particular frequencies where normalized to ω_0 , durations to $T_0 = 2\pi/\omega_0$, electric fields to $E_c = cm_e\omega_0/q_e$ and densities to the critical density n_c . This implies the possibility to scale the frequency of the generated sub-cycle pulses with the input parameters. To increase the output frequency, the input frequency needs to be increased. Moreover, n_e/γ_e has to be increased proportionally and the electron beam duration needs to be decreased. For the cases we are looking at in this Letter, the central frequency up-shifts by about a factor of 10. This leads to the frequency conversion key as presented in Table I.

According to our findings, terahertz (THz) pulses can be used to produce relativistic sub-cycle pulses in the region from mid- to far-IR. We shall discuss the availability of proper seed electromagnetic pulses and electron beams for this proposition. Nowadays, single-cycle THz sources based on organic crystals can reach almost mJ-pulse energies for central frequencies up to $\nu_{\text{THz}} = 4 \text{ THz}$ [16] resulting in relativistic intensities, i.e., reaching peak electric field $q_e E_z^{\text{max}}/(2\pi\nu_{\text{THz}} c m_e) \sim 1$. Sources delivering tens of mJ for $\nu_{\text{THz}} < 3 \text{ THz}$ are in preparation [18]. To obtain sub-cycle pulses of comparable energy, mJ-level electron beam energies are needed. Contemporary laser-wakefield accelerators can provide hundreds of mJ electron beams [14]. In addition, their duration is as short as a few femtoseconds, much shorter than a single THz oscillation, and their charge can be large enough to have a slightly overcritical electron beam for THz frequencies. As we have seen, the single-cycle pulse energies can be larger than the seed pulse energies and thus well above the mJ level. The electric field amplitudes of the amplified pulses can be about one order of magnitude larger than the ones of the seed pulse and thus may reach relativistic intensities.

In summary, we have proposed a scheme for the generation of isolated, intense, sub-cycle pulses which is based on the interaction of an electron beam with a seed electromagnetic pulse reflected by a mirror. The mirror is a crucial element which allows to introduce the electron beam with the correct phase into the fully reflected seed pulse. This ensures an efficient energy conversion from the beam to the pulse leading up to relativistic intensities and down to sub-cycle duration. In particular, we have shown that using currently available intense terahertz pulse sources and laser-wakefield-accelerated electron beams, mJ-strong mid-infrared sub-cycle pulses can be generated. We believe that our proposed scheme will trigger further theoretical and experimental investigations of both, intense sub-cycle pulse sources and applications.

This work was supported by the Knut and Alice Wallenberg Foundation, the European Research Council (ERC-2014-CoG grant 647121) and by the Swedish Research Council, Grant No. 2016-05012. Numerical simulations were performed using computing resources at Grand Équipement National pour le Calcul Intensif (GENCI, Grants No. A0030506129 and No. A0040507594) and Chalmers Centre for Compu-

Seed	frequency	Output	wavelength
THz	1 – 10 THz	(Mid)-IR	3 – 30 μm
(Mid)-IR	10 – 100 THz	Optical	300 nm – 3 μm
Optical	100 – 1000 THz	EUV	30 nm – 300 nm

TABLE I. Frequency conversion key between seed and amplified electromagnetic pulse for the sub-cycle generation mechanism.

tational Science and Engineering (C3SE) provided by the Swedish National Infrastructure for Computing (SNIC, Grant SNIC 2017/1-484, SNIC 2017/1-393, SNIC 2018/1-43).

* illia-thiele@web.de

[1] P. B. Corkum and F. Krausz, *Nat. Phys.* **3**, 381 (2007).

[2] F. Krausz and M. I. Stockman, *Nat. Photonics* **8**, 205 (2014).

[3] M. Hohenleutner, F. Langer, O. Schubert, M. Knorr, U. Huttner, S. W. Koch, M. Kira, and R. Huber, *Nature* **523**, 572 (2015).

[4] T. Rybka, M. Ludwig, M. F. Schmalz, V. Knittel, D. Brida, and A. Leitenstorfer, *Nat. Photonics* **10**, 667 (2016).

[5] M. F. Kling, C. Siedschlag, A. J. Verhoef, J. I. Khan, M. Schultze, T. Uphues, Y. Ni, M. Uiberacker, M. Drescher, F. Krausz, and M. J. J. Vrakking, *Science* **312**, 246 (2006).

[6] C. Hernández-García, J. A. Pérez-Hernández, T. Popmintchev, M. M. Murnane, H. C. Kapteyn, A. Jaron-Becker, A. Becker, and L. Plaja, *Phys. Rev. Lett.* **111**, 033002 (2013).

[7] M. Cristian, M. O. D., C. Giovanni, F. Shaobo, M. Jeffrey, H. ShuWei, H. KyungHan, C. Giulio, and K. F. X., *Laser & Photonics Reviews* **9**, 129 (2015).

[8] H. Liang, P. Krogen, Z. Wang, H. Park, T. Kroh, K. Zawilski, P. Schunemann, J. Moses, L. F. DiMauro, F. X. Krtner, and K.-H. Hong, *Nature Communications* **8** (2017).

[9] D. E. Rivas, A. Borot, D. E. Cardenas, G. Marcus, X. Gu, D. Herrmann, J. Xu, J. Tan, D. Kormin, G. Ma, W. Dallari, G. D. Tsakiris, I. B. Fldes, S.-w. Chou, M. Weidman, B. Bergues, T. Wittmann, H. Schrder, P. Tzallas, D. Charalambidis, O. Razskazovskaya, V. Pervak, F. Krausz, and L. Veisz, *Scientific Reports* **7**, 5224 (2017).

[10] U. Teubner and P. Gibbon, *Rev. Mod. Phys.* **81**, 445 (2009).

[11] E. Esarey, S. K. Ride, and P. Sprangle, *Phys. Rev. E* **48**, 3003 (1993).

[12] S. V. Bulanov, T. Z. Esirkepov, M. Kando, and J. Koga, *Plasma Sources Science and Technology* **25**, 053001 (2016).

[13] Z. Nie, C.-H. Pai, J. Hua, C. Zhang, Y. Wu, Y. Wan, F. Li, J. Zhang, Z. Cheng, Q. Su, S. Liu, Y. Ma, X. Ning, Y. He, W. Lu, H.-H. Chu, J. Wang, W. B. Mori, and C. Joshi, *Nat. Photonics* **1** (2018).

[14] J. P. Couperus, R. Pausch, A. Khler, O. Zarini, J. M. Krmer, M. Garten, A. Huebl, R. Gebhardt, U. Helbig, S. Bock, K. Zeil, A. Debus, M. Bussmann, U. Schramm, and A. Irman, *Nature Communications* **8**, 487 (2017).

[15] J. Derouillat, A. Beck, F. Prez, T. Vinci, M. Chiaramello, A. Grassi, M. Fl, G. Bouchard, I. Plotnikov, N. Aunai, J. Dargent, C. Riconda, and M. Grech, *Computer Physics Communications* **222**, 351 (2018).

[16] C. Vicario, B. Monoszlai, and C. P. Hauri, *Phys. Rev. Lett.* **112**, 213901 (2014).

[17] K. Landecker, *Phys. Rev.* **86**, 852 (1952).

[18] G. Liao, H. Liu, Y. Li, G. G. Scott, D. Neely, Y. Zhang, B. Zhu, Z. Zhang, C. Armstrong, E. Zemaityte, P. Bradford, P. G. Huggard, P. McKenna, C. M. Brenner, N. C. Woolsey, W. Wang, Z. Sheng, and J. Zhang, *arXiv:1805.04369* (2018).